3D Modeling and Simulation of the Thermal Degradation of Composite Material during Space Debris Atmospheric Reentry

Nicolas Perron, Ysolde Prévereaud, Nicolas Dellinger, Marianne J.H. Balat-Pichelin, Julien Annaloro

3D MODELING AND SIMULATION OF THE THERMAL DEGRADATION OF COMPOSITE MATERIAL DURING A SPACE DEBRIS ATMOSPHERIC REENTRY

N. Perron[(1)], Y. Prévereaud[(1)], N. Dellinger[(1)], M. Balat-Pichelin[(2)], and J. Annaloro[(3)]

[(1)]*ONERA/DMPE, F-31055 Toulouse, France, Email: {nicolas.perron, ysolde.prevereaud, nicolas.dellinger}@onera.fr*
[(2)]*PROMES-CNRS, Font-Romeu Odeillo, France, Email: marianne.balat@promes.cnrs.fr*
[(3)]*CNES, Toulouse, France, Email: julien.annaloro@cnes.fr*

ABSTRACT

The spacecraft oriented code ARES developed at ONERA since 2005 to compute Earth and Mars atmospheric reentries is introduced. Then, a new 3D mesh displacement strategy to computed 3D space debris ablation is presented. This strategy is implemented in the material response solver MoDeTheC, which is one of the 4 independant solvers coupled within ARES code. Verification test cases show the capacity of the strategy to deal with important recession and shape changes. This strategy is then used in ARES software to rebuild a wind tunnel ablation test. Finally, the atmospheric reentry of a tank made of an orthotropic composite material is computed, taking into account degradation reaction and shape changes. Two coupling strategy in ARES software are used and compared.

Keywords: atmospheric reentry software; 3D mesh displacement; composite degradation; pyrolysis; oxidation; space debris.

1. INTRODUCTION

Since 1957, thousand of satellites have been launched into space. This human activity has generated a large amount of non functional orbital objects, called "space debris". According to ESA, more than $34\,000$ space debris larger than $10\,\mathrm{cm}$ are in orbit and represent a high risk for the operational satellites in orbit and ground safety. Regarding atmospheric reentry, it is assumed that between $10\,\%$ and $40\,\%$ of the reentering mass (ie. around $32\,000$ tonnes since 1957) already reached the ground. So, the estimation of the total casualty area has become a major issue for all space actors and especially for CNES which is in charge of ensuring the right application of the French Space Operation Law (LOS) by 2021 for French satellites-and-launchers operators and launch operations from French Guyana spaceport.

During an atmospheric entry, space debris are subjected to extreme conditions. A strong shock wave is created in the hypersonic flow where non-equilibrium thermochemical phenomena occur. In this environment, very large heat fluxes are received by the debris. As a consequence, the surface and in-depth material temperatures induce surface and volume material degradation reactions such as oxidation, pyrolysis and fusion/sublimation.

To predict the risk induced by space debris atmospheric reentry, accurate simulations of the material thermochemical degradation are required. Currently, most of the material solvers use 1D, 2D or 2D axisymmetric formulations. However, to be able to cover all kinds of atmospheric entries, a 3D material solver such as PATO [1] or SAMCEF Amaryllis [2] offers better representativeness.

This paper presents the new developments made at ONERA for the computation of composite material degradation during atmospheric reentry. After the description of the in-house ARES code, the new 3D mesh displacement strategy implemented in the material solver MoDeTheC is introduced. Then, an example of composite material degradation during a space debris reentry is presented.

2. ATMOSPHERIC RE-ENTRY SOFTWARE

Atmospheric entry is computed at ONERA with the in-house ARES code (Atmospheric ReEntry Software) where 4 independent solvers are coupled (Fig. 1):

- **MUSIC** (Multi Simulator in Combination) is a space and flight mechanics code able to compute uncontrolled or controlled (Guidance Navigation and Control) trajectory with 3 or 6 degree of freedom;
- **AtMoS** (Atmospheric Models Solver) provides the atmospheric data for Earth (US62, US76, MSIS-00) and Mars entries;
- **FAST** (Fast Aerothermodynamics Solver for Transatmospheric vehicle) is based on analytical models to calculate the heat flux and pressure distributions over an object depending on the farfield condition during the reentry trajectory;

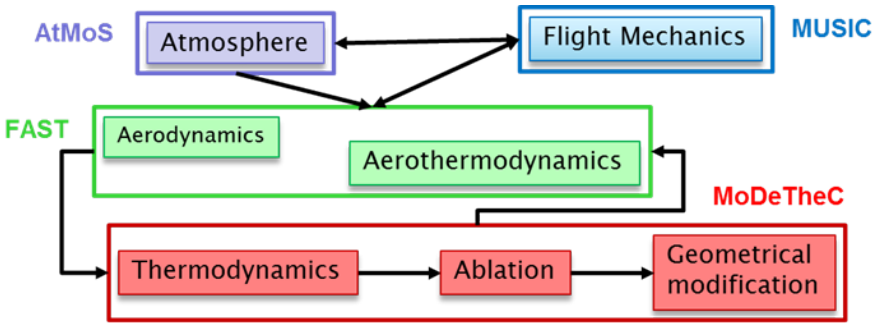

Figure 1: Atmospheric Re-Entry Software: coupling structure of the code

- **MoDeTheC** (for the french "Modélisation de la Dégradation Thermique des Composites") solves the heat and mass transfers as well as thermal degradation within the material.

Within ARES, two options, named one way and two way coupling, are available for the coupling between the solvers FAST and MoDeTheC.

With the one way coupling, the wall temperature of the material is get from the material solver at the beginning of each time step. This wall temperature is used to compute the heat flux and pressure distributions in the solver FAST. The wall heat flux and pressure distribution are then imposed in the material solver MoDeTheC as a boundary condition. With this boundary condition, the heat and mass transfer and the material degradation are computed for the current time step.

With the two way coupling, a radiative equilibrium temperature is sought at the material surface. To do so, the surface energy balance (Fig. 2) is solved with FAST and MoDeTheC solvers:

$$\phi_{conv} + \phi_{diff} + \phi_m + \phi_{rad,in} = \phi_{cond} + \phi_{rad,out} \quad (1)$$

where ϕ_{conv} is the convective heat flux, ϕ_{diff} is the diffusive heat flux, ϕ_m represents the material enthalpy due to species transport, $\phi_{rad,in}$ is the radiative heat flux from the shock layer, ϕ_{cond} is the conductive heat flux in the material and $\phi_{rad,out}$ is the radiative cooling heat flux.

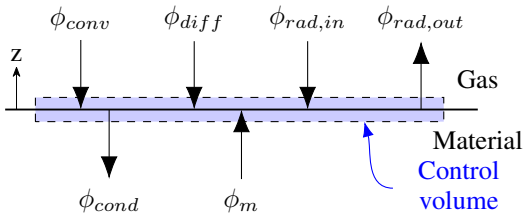

Figure 2: Surface energy balance at an ablative wall

The radiative equilibrium temperature and the pressure found are then imposed in the material solver MoDeTheC as a boundary condition to compute the material degradation.

Currently, material solvers that use 1D, 2D or 2D axisymmetric formulations, cannot model three dimensional space debris accurately. Indeed, 3D objects composed of anisotropic material (carbon composites) and complex structures (sandwich materials with honeycomb core) cannot be reduced to 1D, 2D or 2D axisymmetric formulations. The improvement of ARES ground risk estimation goes through the implementation of a 3D mesh displacement strategy adapted to the finite volume formulation of MoDeTheC.

3. 3D MESH DISPLACEMENT STRATEGY

A new strategy is proposed for managing 3D mesh displacements in order to describe the thermal degradation of materials along an atmospheric reentry. The main objective is to maintain the mesh quality during the ablation process. The strategy was built with the in-house material response code MoDeTheC constraints and must be usable for all possible applications in the atmospheric entry domain. The main constraints to respect are:

- to define a unique strategy for any kind of mesh type (structured, unstructured and hybrid),
- to be relevant to any kind of object shape,
- to automatically detect the surface to ablate without preliminary identification, since in case of space debris atmospheric entry the surface recession can occur anywhere.

The proposed mesh displacement strategy is performed in three steps detailed in Fig. 3 and each step is described hereafter.

3.1. Moving surface mesh method

To properly move the vertices where ablation occurs, the moving surface mesh method is based on the automatic classification of the mesh vertices according to their belonging to one, two or three surfaces (plane or curved). So, vertices located on one surface define what is called the "surface vertices" while vertices located at the intersection between two surfaces defining the "curves" of the

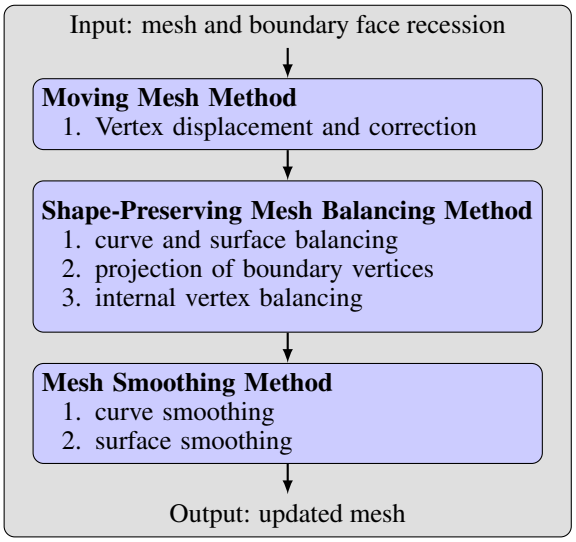

Figure 3: Mesh displacement strategy

computational domain are called "curve vertices". Finally, vertices at the intersection between three surfaces are called "corner vertices".

For each boundary vertex, the vertex displacement method is divided into 3 steps:

1. For each (1, 2 or 3+) surface around the vertex, an equivalent displacement velocity is calculated as the average of the ablation velocity of the nearby faces belonging to the studied surface weighted by their surface area.
2. A correction is applied to each equivalent displacement velocity to keep vertices in the domain.
3. The corrected equivalent displacements are summed to access to the final vertex displacement.

Deformed during this step, the new object shape must be maintained during the following steps.

3.2. Shape-preserving mesh balancing method

Because the mesh displacement strategy in MoDeTheC is based on an Arbitrary Lagrangian-Eulerian formulation, boundary and internal vertices must be balanced to prevent mesh cell inversion while preserving the object shape. The procedure is divided into 4 steps:

1. The curve vertices are balanced by applying a Laplacian smoothing. To prevent high shape modifications, the vertex displacement is reduced to the edges composing the curve.
2. The surface vertices are balanced by applying a Laplacian smoothing. For the same reason as curve vertices, the surface vertices displacements are reduced to the faces of the object surface.
3. The balanced curve and surface vertices are projected respectively on the tangent line and plane at the initial vertex location.
4. The internal vertices are balanced with a Laplacian smoothing.

3.3. Mesh smoothing method

During the computation, high frequency oscillations of the mesh can be observed. This issue is solved by applying a smoothing step on boundary curves and surfaces. The smooth curves and surfaces are defined by implicit polynomial equations obtained by a weighted least square method.

4. VERIFICATION AND VALIDATION OF THE 3D MESH DISPLACEMENT STRATEGY

The implementation of the 3D mesh displacement strategy in MoDeTheC was verified on many 2D and 3D shapes. In this section, two test cases initially proposed in 2D by Droba [3] are reproduced and extended to 3D cases. Then, the wind tunnel experiment on camphor sublimation made by Baker [4] is rebuilt with ARES.

4.1. Sinusoidal slider

The need of the projection step during the Shape-Preserving Balancing step can be shown with the sinusoidal slider test case of Droba [3]. The sinusoidal geometry is meshed with GMSH. The structured mesh, composed of 600 elements, is shown in Fig. 4a.

An ablation velocity $\mathbf{V}_{imp} = 0.01\,\mathrm{m/s}$ is set on the left boundary surface (Fig. 4a) during the $250\,\mathrm{s}$ computation with a time step $\delta t = 0.05\,\mathrm{s}$. For this case, no heat or mass transfer are taken into account. The material properties are therefore not given as they do not alter the result.

The boundary vertices projection prevents the sinusoidal shape from changing during the computation, up to $t = 250\,\mathrm{s}$ (Fig. 4) whereas the wave shape is quickly flattened without projection.

The 2D sinusoidal slider is extruded to demonstrate the shape preservation in 3D (Fig. 5). The solution at successive moments show that the upper wavy surface is ablated without affecting the initial sinusoidal shape.

4.2. Receding rectangle

The ability of MoDeTheC to manage important shape changes is demonstrated with the next verifications. The heat flux is high at sharp edges during atmospheric reentry due to a small curvature radius. Corner and sharp edges are blunted as a consequence. The receding rectangle computations illustrate this capacity in 2D and 3D.

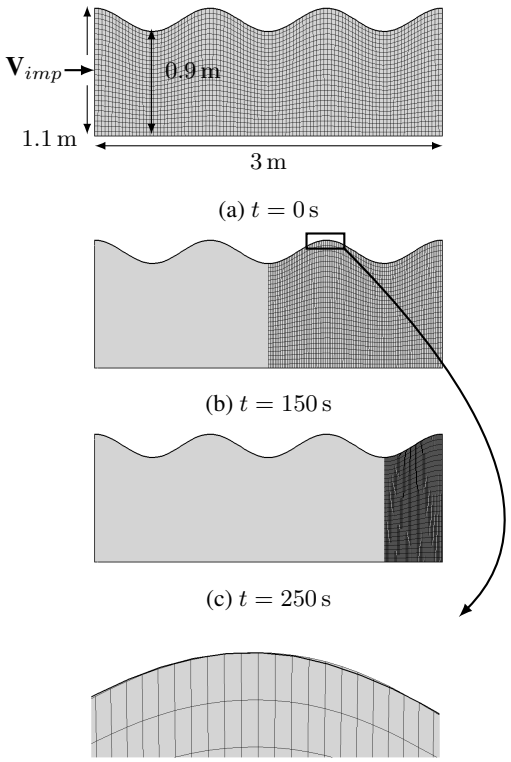

(a) $t = 0\,\mathrm{s}$

(b) $t = 150\,\mathrm{s}$

(c) $t = 250\,\mathrm{s}$

(d) zoom at $t = 150\,\mathrm{s}$

Figure 4: 2D sinusoidal slider ablation

These computations apply a sublimation model contrary to previous tests performed with an imposed ablation velocity. A sublimation temperature T_{sub} and a sublimation enthalpy ΔH_{sub} are defined, eventually as a function of the wall pressure. During a computational time step, the energy received at the material surface E_w might lead to a surface temperature higher than the sublimation temperature. In this case, the incoming energy is reduced to E'_w for which the surface temperature will match the sublimation temperature. This energy difference $E_w - E'_w$ corresponds to the energy necessary to sublimate the material.

The material properties are:

- Density: $\rho = 2000\,\mathrm{kg/m^3}$
- Heat capacity: $C_P = 1000\,\mathrm{J/(kg\cdot K)}$
- Thermal conductivity: $k = 0.4\,\mathrm{W/(m\cdot K)}$
- Sublimation temperature: $T_{sub} = 1000\,\mathrm{K}$
- Sublimation enthalpy: $\Delta H_{sub} = 205\,000\,\mathrm{J/kg}$
- Initial temperature: $T_i = 500\,\mathrm{K}$

The same heat flux $\phi = 4\,\mathrm{MW/m^2}$ is imposed on the 2D receding rectangle boundaries Γ_1 and Γ_2 whereas a null heat flux is applied to Γ_3 and Γ_4 (Fig. 6).

The thermal response is plotted at 3 instants. Sharp boundary vertices are marked by red squares whereas the other boundary vertices are not marked. At $t = 50\,\mathrm{s}$, the upper left corner vertex color goes from red to no mark. This means that the corner vertex is blunted as expected

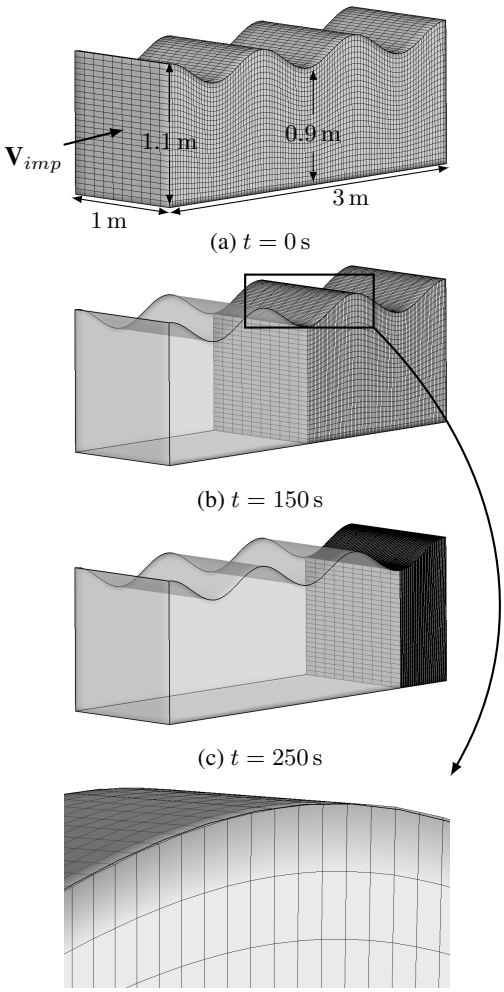

(a) $t = 0\,\mathrm{s}$

(b) $t = 150\,\mathrm{s}$

(c) $t = 250\,\mathrm{s}$

(d) zoom at $t = 150\,\mathrm{s}$

Figure 5: 3D sinusoidal slider ablation

for such material exposed to atmospheric reentry equivalent conditions.

A similar computation is done in 3D (Fig. 7) with an extrusion of the 2D case. The same heat flux ϕ is imposed on the boundary surfaces Γ_1 and Γ_2. Boundary vertices are marked in red for the corner vertices and in green for curve vertices. At $t = 50\,\mathrm{s}$, the boundary curve between Γ_1 and Γ_2 is blunted and the other object shape features are preserved.

4.3. Spherically-blunted cone sublimation

The validation of the ablation model in ARES is done with material whose ablation is only due to sublimation. This removes the many physical and chemical phenomena occurring during an atmospheric reentry and thus reduces the uncertainties. For this reason, the ablation validation is performed with low temperature ablators like dry ice or camphor.

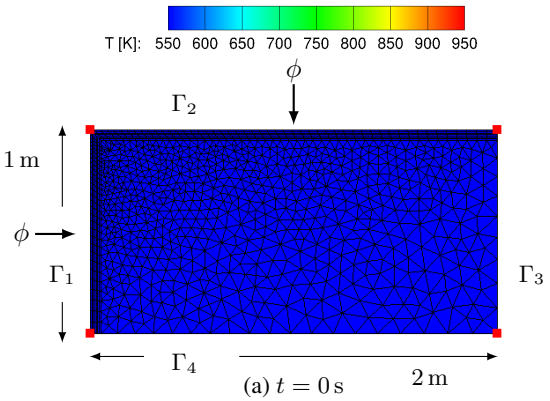

(a) $t = 0\,\mathrm{s}$

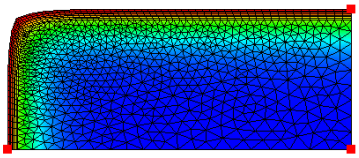

(b) $t = 300\,\mathrm{s}$

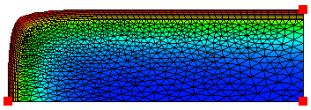

(c) $t = 500\,\mathrm{s}$

Figure 6: 2D receding rectangle ablation

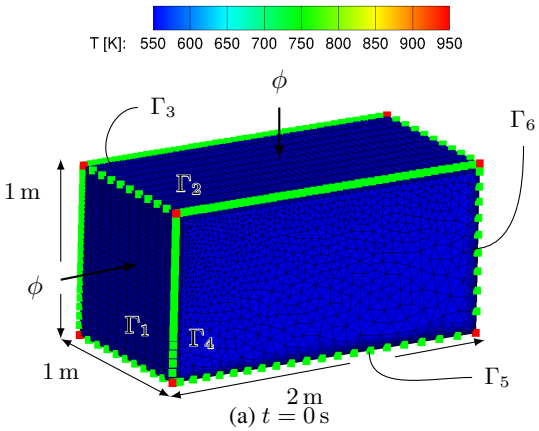

(a) $t = 0\,\mathrm{s}$

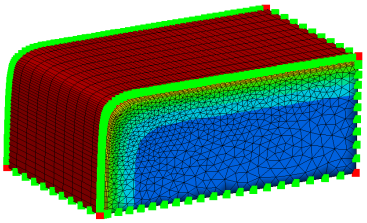

(b) $t = 300\,\mathrm{s}$

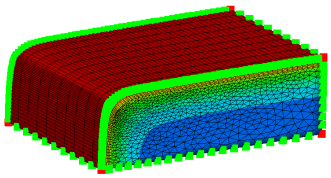

(c) $t = 500\,\mathrm{s}$

Figure 7: 3D receding rectangle ablation

In this section, the wind tunnel experiment made by Baker [4] on camphor sublimation is presented. A spherically-blunted cone (Fig. 8) of $6.35\,\mathrm{cm}$ radius, $24\,\mathrm{cm}$ length and a $8°$ half-angle cone is used. This sample is exposed to a Mach 5 laminar flow during $320\,\mathrm{s}$. The freestream condition of the wind tunnel are: $\rho = 0.04\,\mathrm{kg/m^3}$, $T = 132\,\mathrm{K}$ and $V = 1155\,\mathrm{m/s}$.

This wind tunnel experiment is rebuilt with the ARES software, using only FAST and MoDeTheC solvers. These solvers are coupled with the one way coupling approach described in section 2. Centaur software is used to generate an unstructured mesh composed of 87 000 cells with prism layers near the surface and tetrahedra elsewhere.

Camphor material is defined is ARES with the properties in [5]:

- Density: $\rho = 990\,\mathrm{kg/m^3}$
- Heat capacity: $C_P = 1863\,\mathrm{J/(kg\cdot K)}$
- Thermal conductivity: $k = 0.4\,\mathrm{W/(m\cdot K)}$

The camphor sublimation is computed with the Latent Enthalpy ablation method of Mullenix [9]. The pressure-

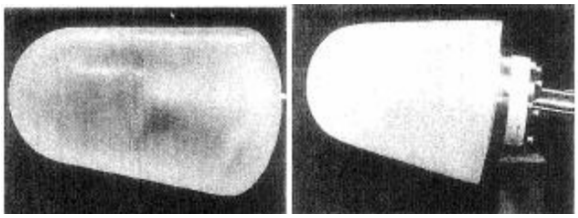

Figure 8: Camphor samples used for wind tunnel experiments [4]

temperature sublimation equation is modelled with the Antoine-like equation:

$$p = 10^{A-B/(T+C)} \tag{2}$$

where p is the pressure (in Torr) and T is the temperature (in °C). The three coefficients of the Antoine equation are found from experimental data [6]: $A = 8.52$, $B = 2714.91$ and $C = 277.67$. The sublimation enthalpy of camphor is constant for this computation and equal to $0.341\,\mathrm{MJ/kg}$.

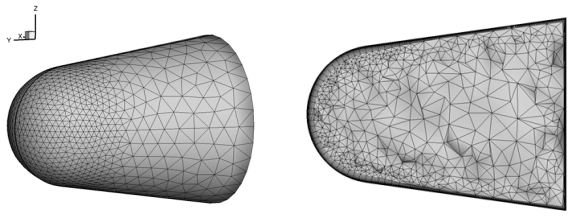

Figure 9: Mesh of the spherically-blunted cone used for ARES computation

ARES is run during 320 s with a constant time step of 0.005 s. The initial material temperature during the experiment is not given and is assumed to be 298.15 K as in Bianchi and Turchi [6] computations.

A cross-sectionnal view of the temperature field after the 320 s of simulation is shown in Fig. 10. The initial boundary mesh is shown in the background to highlight the important surface recession: a 5 cm recession compared to the 24 cm initial length. This computation proves the capacity of ARES to maintain the mesh quality during the ablation process. This is especially important near the boundary where the prism layer size is constant.

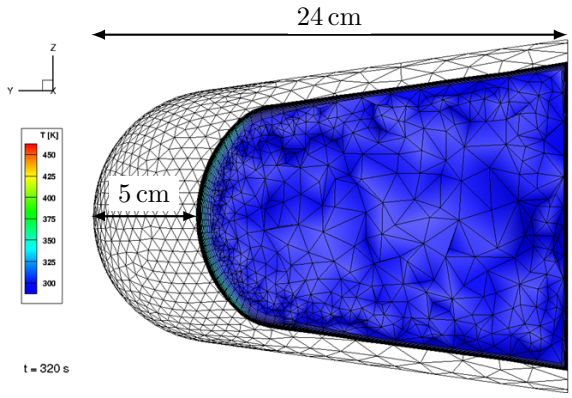

Figure 10: Temperature field in the cross-sectionnal view of the camphor geometry after the 320 s computation

ARES result is compared to Baker experimental and computational results in Fig. 11. The boundary recession of ARES computation is close to Baker results up to 200 s. However, at 320 s, ARES overestimates the recession. This difference might be due to the blowing of sublimation gases which reduces the heat flux at the material wall. This blowing effect is accounted for by Baker with the corrected Stanton number due to mass addition whereas this effect is currently not modelled in ARES.

The verification test cases and the computation of camphor sublimation proves the capacity of the 3D mesh displacement strategy of MoDeTheC to deal with important shape changes during an ablation process. In ARES software, this feature can be used to compute the atmospheric reentry of space debris made of various material. The example of the atmospheric reentry of a composite tank is presented in the next section.

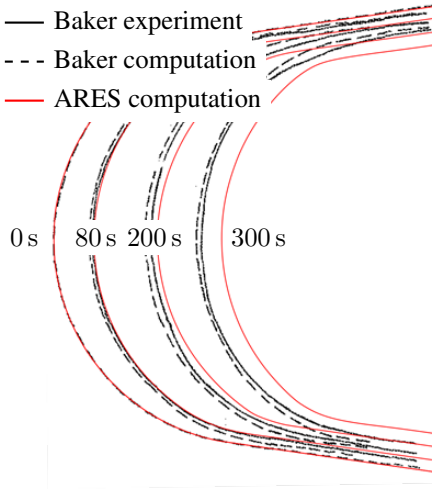

Figure 11: Comparison of camphor shapes at different solution time

5. COMPOSITE TANK REENTRY

In this section, the atmospheric reentry of a composite tank, similar to the one presented in Fig. 12, found in India, is performed.

Figure 12: Tank found close to Dindigul, India [8]

For this computation, the shape of the composite tank is modelled by a hollow sphere of 1 m diameter and 4 mm thickness. This geometry is meshed using GMSH with prism layers. The resulting mesh of Fig. 13 is composed of 24 000 cells.

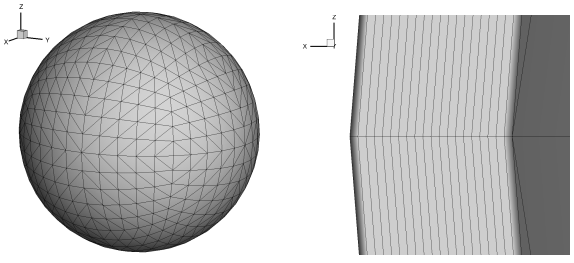

(a) (b)

Figure 13: 3D mesh of the hollow sphere: (a) boundary and (b) prism layer views

The composite material chosen for this test case is the T700M21, a carbon epoxy characterized by Biasi [7] at ONERA. This aeronautical composite is first used because the material properties are available. It will then be replaced by an aerospace composite manufactured and used by Thales Alenia Space once its characterisation will be completed.

Because the material solver MoDeTheC is implemented with a multi-component formulation, the T700M21 is defined with four components: the carbon fibers, the epoxy matrix, the char and the decomposition gas (DG). The T700M21 component properties are shown in Tables 1 and 2. As the solid properties were determined between $300\,\mathrm{K}$ and $400\,\mathrm{K}$, the solid component properties are set as temperature independent to avoid large extrapolation at high temperature. In the composite material, the thermal conductivity has an orthotropic behaviour. To model it, the thermal conductivity is set to $0\,\mathrm{W/(m\cdot K)}$ in the transverse direction of the fibers, *i.e.* the radial direction in spherical coordinates.

Table 1: Solid component physical properties

	Fibers	Matrix	Char
Density $\left[\mathrm{kg/m^3}\right]$	1800	1280	1489
Specific heat $[\mathrm{J/(kg\cdot K)}]$	1200	1720	2900
Thermal conductivity $[\mathrm{W/(m\cdot K)}]$	$k_\theta = 11.5$ $k_r = 0$	0.194	19.7
Surface emissivity	0.808	0.912	0.808

Table 2: Decomposition gas physical properties

	DG
Molar mass $[\mathrm{g/mol}]$	15.57
Dynamic viscosity $[\mathrm{Pa\cdot s}]$	$2E-5$
Specific heat $[\mathrm{J/(kg\cdot K)}]$	$f_1(T)$
Thermal conductivity $[\mathrm{W/(m\cdot K)}]$	$f_2(T)$

with $f_1(T) = 1972.5 + 1.45T + 9.59\times10^{-4}T^2 + 3.47\times10^{-7}T^3$, $f_2(T) = 2.88E-2 + 7.74\times10^{-5}T$ and T the temperature (in K).

The thermal decomposition of the T700M21 composite material is modelled with 3 successive degradation reactions (Fig. 14). First, the epoxy matrix is transformed into a carbon residue (char) and a decomposition gas. The char is then oxidised due to the interaction with the air atmosphere. After this first oxidation, the carbon fibers are the last component and are also oxidised. These three reactions are modelled with Arrhenius laws. The law parameters are found with experiments (ThermoGravimetric Analysis and Differential Scanning Calorimetry) and are summarized in table 3.

Table 3: Arrhenius law parameters

	Pyrolysis	Oxidation 1	Oxidation 2
$\nu\,[-]$	0.45	–	–
$A\,[1/\mathrm{s}]$	9.03×10^5	5.62×10^{10}	2.0×10^5
$E_A\,[\mathrm{J/kg}]$	1.055×10^5	2.033×10^5	1.677×10^5
n	1.8	1.8	0.5

with ν the stoichiometric mass coefficient of the solid product, A and E_A are respectively the pre-exponential factor and the activation energy of the Arrhenius law, and n is the order of reaction.

The atmospheric reentry computation with ARES is started at the fragmentation altitude $h = 78\,\mathrm{km}$ with an initial velocity $V_i = 7\,\mathrm{km/s}$ and an flight path angle $\gamma = -0.1°$. The initial material properties are the temperature $T_i = 300\,\mathrm{K}$ and volume fractions $\phi_{fibers} = 0.569$, $\phi_{matrix} = 0.419$ and $\phi_{DG} = 0.012$. The initial mass of the computed composite tank is $19.45\,\mathrm{kg}$.

The reentry computation is run with a time step $\delta t = 0.01\,\mathrm{s}$ with a 3 degree of freedom model for the flight mechanics (MUSIC) and the US76 atmosphere model (AtMoS). The internal wall of the hollow sphere is an adiabatic wall and both the one way and two way couplings are evaluated.

The reentry computational result for the one way coupling is shown in Fig. 15. Due to the low ballistic coefficient of the tank, the reentry is slowed down quickly (Fig. 15b). The convecto-diffusive heat flux at the material wall is thus decreasing from $0.5\,\mathrm{MW/m^2}$ at $78\,\mathrm{km}$ to $0\,\mathrm{MW/m^2}$ at $47\,\mathrm{km}$. Between these altitudes, the wall temperature at the stagnation point reaches a maximum of $1330\,\mathrm{K}$ at $74\,\mathrm{km}$ (Fig. 15c). The heat flux entering in the material increases the internal temperature of the composite and the degradation reactions are activated. At $47\,\mathrm{km}$, $40\,\%$ of the material thickness at the stagnation point is fully pyrolysed. The oxidation of the char starts in all the thickness but only $10\,\%$ of the thickness completes this degradation reaction. The oxidation of the fibers occurs only at the material surface, when all the char is oxidised. Due to the small amount of energy received by the tank during the reentry, the recession reaches only $0.18\,\mathrm{mm}$ at the stagnation point. After $47\,\mathrm{km}$, when the surface cools down, the oxidation reactions are stopped. Only the pyrolysis of the matrix continues to degrade the composite.

The reentry computation with the two way coupling leads to similar results. The main differences are shown in Fig. 16. With the two way coupling (radiative equilibrium), the wall temperature resulting from the surface energy balance is found to be higher than with the one way coupling (Fig. 16a). For the one way coupling, the wall temperature plotted in Fig. 16a is the one extrapolated in the material solver from inner temperatures.

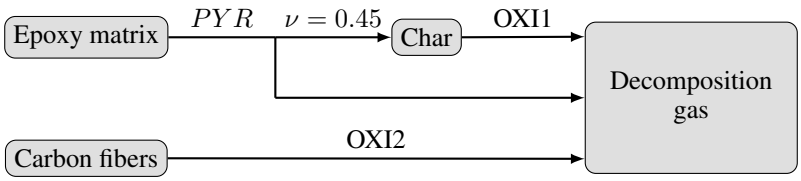

Figure 14: Reaction mechanism of the T700M21 thermal degradation

Because the wall temperature is higher for the two way coupling, the radiative cooling heat flux is also higher. The convecto-diffusive heat flux is similar whatever the coupling method because it is less temperature-dependent than the radiative heat flux of the wall. The energy entering the material during the atmospheric reentry is therefore higher with the one way coupling. As a consequence, the degradation reactions with the two way coupling are delayed and less extended at the end of the reentry. For example, the oxidation of the fibers removes only $0.3\,\%$ of the material thickness in two way coupling whereas $4.4\,\%$ are removed with the one way coupling.

6. SUMMARY AND FURTHER WORK

The software developed at ONERA to compute Earth and Mars atmospheric reentries (ARES) was presented with its four independent codes. Two options for the coupling between the fluid and the material solvers were introduced. Then, the new 3D mesh displacement strategy to compute space debris ablation in the material solver MoDeTheC was introduced. This capacity can be used with the independent material solver MoDeTheC and within the atmospheric reentry software ARES. The 3D mesh displacement strategy implemented in MoDeTheC was successfully verified on geometrical test cases to prove the capacity to manage important recession and shape changes. Then, the comparison between wind tunnel ablation test and ARES computation shows first quantitative results which will be improved by adding physical phenomena (blowing effects).

Finally, the atmospheric reentry of the tank proves the capacity of ARES software to couple the 3D material response code MoDeTheC with the fluid analytical solver FAST during an atmospheric reentry. This coupling allows to compute on the one hand internal degradation reactions like pyrolysis and char oxidation and on the other hand surface degradation reactions like fiber oxidation. These reactions are computed during an atmospheric reentry trajectory and modify the composition, the properties and the shape of the tank.

Further work consists first in the characterization of a spatial carbon epoxy material manufactured and used by Thales Alenia Space. This composite will replace the T700M21 in the reentry computation. Some inputs of the reentry computation could also be modified to add complexity in the reentry test case (drilling of the tank, 6 DOF). Finally, the effect of pyrolysis and oxidation gases on the convecto-diffusive heat flux will be studied.

ACKNOWLEDGMENTS

This work was supported by the ONERA and "Centre National d'Études Spatiales" (French Space Agency) through the co-funding of the PhD of N. Perron.

REFERENCES

1. Lachaud, J., Mansour, N. M., (2014). Porous-Material Analysis Toolbox Based on OpenFOAM and Applications, *Journal of Thermophysics and Heat Transfer*
2. http://www.sigmeo.fr/samcef, Accessed 3 November 2020
3. Droba, J., (2016). Tangle-free Finite Element Mesh Motion for Ablation Problems, *46th AIAA Thermophysics Conference*
4. Baker, R. L., (1972). Low Temperature Ablator Nosetip Shape Change at Angle of Attack, *AIAA 10th Aerospace Sciences Meeting*
5. Charwat A. F., (1958), Exploratory Studies on the Sublimation of Slender Camphor and Naphthalene Models in a Supersonic Wind-Tunnel
6. Bianchi D., Turchi A., (2019), Numerical analysis on the sublimation low-temperature ablator models undergoing shape change in a supersonic wind-tunnel, *8th European Conference for Aeronautics and Aerospace Sciences*
7. Biasi V., (2014), Modélisation thermique de la dégradation d'un matériau composite soumis au feu, PhD thesis, ISAE - Toulouse
8. Bastida Virgili B., Lemmens S., Siminski J., Funke Q., (2017), Practicalities of re-entry predictions – the VEGA-01 AVUM case
9. Mullenix N., (2005), A coupled gas dynamics and heat transfer method for simulating the laser ablation process of carbon nanotube production, PhD thesis

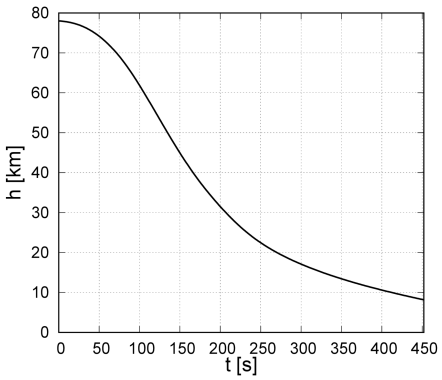

(a)

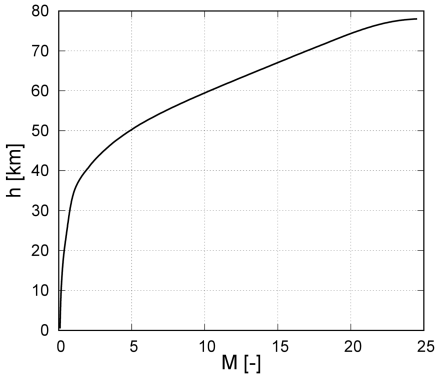

(b)

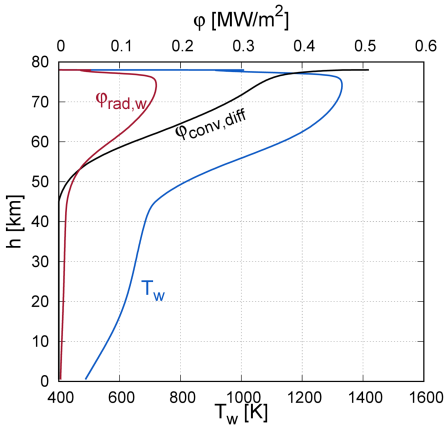

(c)

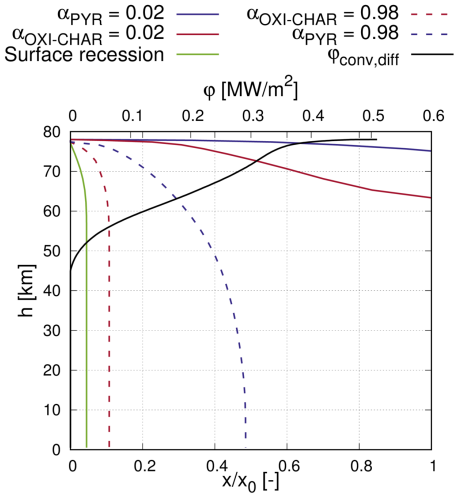

(d)

Figure 15: Atmospheric entry of the composite tank with the one way coupling

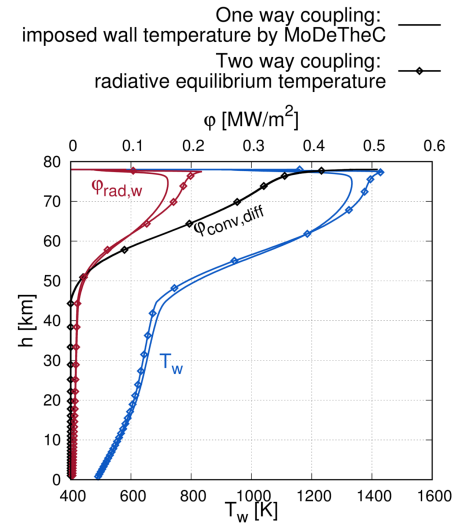

(a)

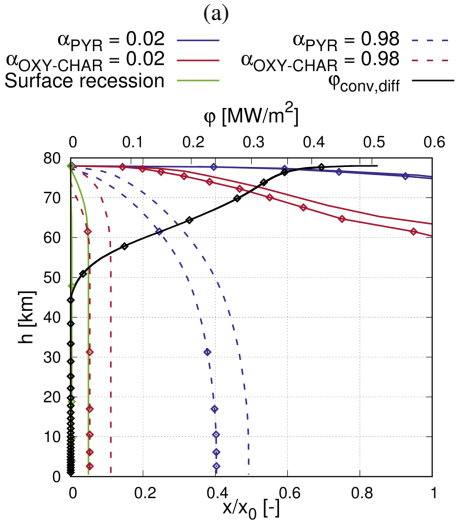

(b)

Figure 16: Comparison of the atmospheric reentry of the composite tank between the one way and the two way coupling